Dalton Transactions

Accepted Manuscript

ROYAL SOCIETY OF CHEMISTRY

www.rsc.org/dalton

Journal Name

ARTICLE TYPE

Cite this: DOI: 10.1039/xxxxxxxxxx

Vibrational circular dichroism and chiroptical properties of chiral Ir(III) luminescent complexes †,¶

Giuseppe Mazzeo[a,‡], Marco Fusè[b,‡], Giovanna Longhi[a,c], Isabella Rimoldi[b], Edoardo Cesarotti[b], Alessandra Crispini[d], Sergio Abbate*[a,c]

Received Date
Accepted Date

DOI: 10.1039/xxxxxxxxxx

www.rsc.org/journalname

The octahedral ionic Ir(III) complex with a dual stereogenic centre of general formula Δ,Λ-*(R,S)*-[(ppy)$_2$Ir(Me-campy)]X, where ppy=2-phenylpyridine, Me-campy=2-methyl-5,6,7,8-tetrahydroquinolin-8-amine, and the complex Λ-*(R,S)*-[(ppy)$_2$Ir(H-Campy)]X, where ppy=2-phenylpyridine, H-Campy=8-amino-5,6,7,8-tetrahydroquinolines and with X$^-$ = Cl$^-$ as counterion in both cases, have been characterized by vibrational circular dichroism (VCD), which turns out to be efficacious in diastereomeric discrimination. Moreover, the single crystal X ray structure of complex Δ-*(R)*-[(ppy)$_2$Ir(Me-Campy)]Cl is reported. Density functional theory (DFT) calculations allow to understand that the most important doublet feature in the VCD spectra associates with a clear vibrational exciton structure located on the two dissymetrically disposed phenylpyridine ligands. The features in the VCD spectra associated with the *(R)* or *(S)*-central chirality configuration are identified and commented. DFT calculations provide also the interpretation of electronic circular dichroism (ECD) spectra. Finally circularly polarized luminescence (CPL) spectra are presented as an additional chiroptical characterization of these luminescent iridium complexes.

1 Introduction

Cyclometallated Ir(III) complexes have been extensively studied in the last years due to their extraordinary photophysical properties associated to their MLCT transitions[1]: large Stoke shift, tunability of the absorption and emission wavelength, high phosphorescent quantum yields with high quantum efficiency made them attractive for application in several fields[2–4]. Due to the properties reminded above, they proved also to be effective in the biological sphere for the development of labelling, sensing or bioimaging devices[5–12]. The Ir(III) complexes studied here are characterized by an inert inner coordination sphere with a stereogenic metal centre. For use in biomolecular recognition applications, the resolution of the enantiomers Λ and Δ can be necessary[6]. Contrary to the related Ru(bipy)$_3^{2+}$ complexes, the separation of the enantiomers is still a challenge; usually it is achieved by co-crystallization with a chiral counter anion[13] or by HPLC with a chiral ligand[14,15] or chiral stationary phase[16]. In this context the certain definition of the stereochemistry plays a crucial role. Recently we synthesized octahedral ionic Ir(III) complexes with a dual stereogenic centre of general formula Δ,Λ-*(R,S)*-[(ppy)$_2$Ir(Me-Campy)]X, where ppy=2-phenylpyridine, Me-Campy=2-methyl-5,6,7,8-tetrahydroquinolin-8-amine, and the complex Λ-*(R,S)*-[(ppy)$_2$Ir(H-Campy)]X, where H-Campy=8-amino-5,6,7,8-tetrahydroquinolines and with X$^-$ = Cl$^-$ as counterion (see **Scheme 1**).[17] Hereafter we call the first set of compounds Ir-Me-Campy and the second set Ir-H-Campy. Complexes were synthesized starting from the splitting reaction of the [Ir(ppy)$_2$(μ-Cl)]$_2$ dimer with two equivalents of the optically pure chiral diamine. The diastereomers were thus separated by selective precipitation after metathesis reaction with (+)-10-camphorsulfonate. The main focus of this work will be on the chiroptical properties of these kinds of complexes, with special emphasis on vibrational circular dichroism (VCD). VCD technique in association with density functional theory calculation (DFT) has reached considerable achievements in assigning the absolute configuration (AC) and the conformational properties of many molecular systems, including drugs, peptides, proteins, molecular

[a] *Dipartimento di Medicina Molecolare e Traslazionale, Università di Brescia, Viale Europa 11, 25123 Brescia, Italy; Fax: +39 030 3701157; Tel: +39 030 3717415; E-mail: sergio.abbate@unibs.it*
[b] *Dipartimento di Scienze Farmaceutiche, Università di Milano Via Golgi 19, 20133 Milano, Italy*
[c] *CNISM Consorzio Nazionale Interuniversitario per le Scienze Fisiche della Materia,Via della Vasca Navale, 84, 00146 Roma, Italy*
[d] *Centro di Eccellenza CEMIF.CAL-LASCAMM, CR-INSTM (Unità della Calabria, Dipartimento di Chimica e Tecnologie Chimiche) University of Calabria, I-87030 Arcavacata di Rende (CS), Italy;*
† Electronic Supplementary Information (ESI) available: [details of any supplementary information available should be included here]. See DOI: 10.1039/b000000x/
‡ These authors contributed equally to this work
¶ Work presented at EuCOMC, Bratislava, Slovakia, July 2015

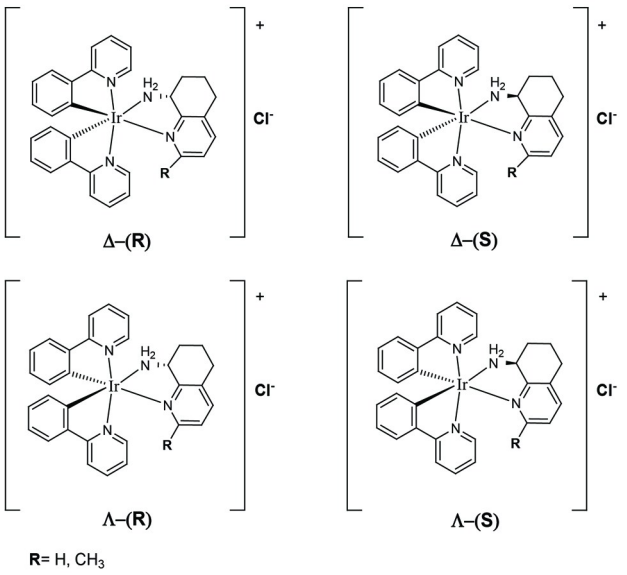

Scheme 1 Chemical Structures of the Ir(III) complexes examined in the present study.

aggregates[18–24] and metallo-organic complexes.[25–28] From VCD data analysis we gain information on the metal chirality and on ligand chirality, whose effect is obscured by chirality at the metal in electronic circular dichroism (ECD) data.[17] The fact that this goal can be achieved by VCD was strongly suggested by previous instances in which we were able to disentangle axial or planar chirality from central chirality.[29,30] The X-ray results reported below will leave no doubt to configurational assignment. Finally due to the luminescent properties of these Ir(III) complexes we also investigated circularly polarized luminescence (CPL)[16,31,32] and we are able to establish whether luminescence properties depend on both types of stereogenic sources and how large are the chiral manifestations in emission.

2 Experimental

2.1 Materials and Methods

Ir(III) chloride hydrate ($IrCl_3 \cdot xH_2O$) was purchased from Alfa Aesar. Reagents and all the solvents were purchased from commercial sources and used without further purification. Complexes were synthesised and the diastereoisomeric mixture separated as reported in ref.[17] and references therein. ^{1}H NMR spectra were recorded in $CDCl_3$, CD_3OD or a mixture of them on either a Bruker DRX Avance 300 MHz apparatus equipped with or a nonreverse probe or Bruker DRX Avance 400 MHz apparatus. Chemical shifts (in ppm) were referenced to residual solvent proton peak (see **ESI-1**).

2.2 X-ray crystallographic analysis

Single crystal data of Ir-Me-Campy were collected at room temperature with a Bruker-Nonius X8APEXII CCD area detector system equipped with a graphite monochromator with radiation Mo Kα (λ = 0.71073 Å). Data were processed through the SAINT[33] reduction and SADABS[34] absorption software. The structure was solved by direct methods through the SHELXTL-NT[35] structure determination package and refined by full-matrix least-squares based on F^2. All non-hydrogen atoms were refined anisotropically and hydrogen atoms were included as idealized riding atoms. Hydrogen atoms of the co-crystallized water molecules have been included in calculated positions and restrained bond distances and angles have been used. The final geometrical calculations and the graphical manipulations were performed using the XP utility of the SHELXTL system. Cell parameters and final refinement data are given in **ESI-2**. Selected interatomic bond lengths and angles are given in **Table 1**. CCDC reference number is 1414409. See electronic supporting information for crystallographic data in CIF.

Table 1 Selected distances (Å) and angles (°) in Δ*R*-Ir-Me-Campy

Ir-C(11)	2.021(4)	N(2)-Ir-N(4)	89.9(1)
Ir-C(22)	2.031(4)	N(3)-Ir-N(4)	76.6(1)
Ir(1)-N(1)	2.057(3)	C(11)-Ir-C(22)	86.0(1)
Ir(1)-N(2)	2.071(3)	C(11)-Ir-N(1)	80.5(1)
Ir(1)-N(3)	2.189(3)	C(11)-Ir-N(2)	95.8(1)
Ir(1)-N(4)	2.252(3)	C(11)-Ir-N(3)	95.7(1)
		C(11)-Ir-N(4)	170.9(1)
N(1)-Ir-N(2)	174.4(1)	C(22)-Ir-N(1)	95.5(1)
N(1)-Ir-N(3)	88.1(1)	C(22)-Ir-N(2)	80.0(1)
N(1)-Ir-N(4)	94.4(1)	C(22)-Ir-N(3)	176.3(1)
N(2)-Ir-N(3)	96.5(1)	C(22)-Ir-N(4)	102.1(1)

2.3 VCD and IR (Vibrational Absorption = VA) Spectra

All spectra were taken with a Jasco FVS6000 VCD spectrometer with liquid N_2-cooled MCT detector. Spectra were taken at room temperature (25°C) for CD_2Cl_2 solutions in the range 0.027-0.037 M concentration, in 200 μm BaF_2 cells. In some cases a drop of CD_3OD was added to the solution, to facilitate dissolving the sample. Repeated sets of 2000 scans were taken for each sample and spectra were co-added, when needed; subtraction of VA and VCD spectra of the solvent were performed.

2.4 ECD and UV Spectra

Spectra were taken with a Jasco 815SE spectrometer and 2 mm quartz cells were employed; with CD_2Cl_2 solutions in concentration range from 0.00023 M to 0.00026 M. Spectra were taken at 25°C.

2.5 CPL Spectra

Spectra were taken with a home-built apparatus described in ref.[36–38] with excitation radiation brought in through an optical fibre from a Jasco FP8200 fluorimeter. The same solution used for the ECD spectra was employed for CPL measurements. Five scans were accumulated for each spectrum. The excitation wavelength has been 380 nm. The Fluorescence spectra reported in this work are those simultaneously taken with the same non-commercial apparatus. All spectra were were taken at 25°C.

2.6 Density Functional Theory (DFT) Calculations

DFT calculations were conducted with the module of Gaussian09,[39] which was run at the B3LYP/6-31+G(d,p) level of theory; the LANL2DZ pseudopotential was used for the Ir atom[40–42]. The input geometry was taken from X-ray diffraction data and then optimized with due allowance of solvent in the PCM polarizable continuum model approximation[43]. Calculation of Dipole and Rotational Strengths through the field-response approach[44] was carried out; VA and VCD spectra were generated by assigning 8 cm^{-1} bandwidth Lorentzian bandshape to each vibrational transition. In all cases we also allowed for the presence of one Cl^- counterion. The scaling factor 0.975 was applied to the calculated frequencies. Time-Dependent DFT (TDDFT) calculations have been employed, within the same Gaussian package, to obtain ECD spectra: the same level of theory was adopted and 40 excited states were admitted. Spectra were then plotted by associating Gaussian bands to each transition with 0.15 eV bandwidth.

3 Results and Discussion

As stated above, the goal of the present work is the study of chiroptical properties of molecules reported in **Scheme 1**. However an important prerequisite to perform DFT calculations useful to the interpretation of CD spectra is the knowledge of the 3D-structure: this is achieved on Ir-Me-Campy by single crystal X-ray.

3.1 Structural description from single crystal X-ray results

As shown in **Figure 1** the iridium(III) metal centre in the cationic complex of Ir-Me-Campy is hexa-coordinated with achiral bidentate ligands, two cyclometalated ppy, and the chiral Me-Campy ancillary ligand. Complex Ir-Me-Campy crystallizes in the orthorhombic enantiomorphic space group P2(1)2(1)2(1). The absolute configuration has been also determined, and corresponds to the Δ form. Several crystals of Ir-Me-Campy have been tested, but we never found racemic crystals, proving that the enantiomeric separation successfully occurred from the specific metathesis reaction.[17] The asymmetric unit of Ir-Me-Campy is made up of a single cationic complex, exhibiting a distorted octahedral geometry around the Ir(III) metal centre, and one co-crystallized water molecule. The two ppy adopt the usual NN *trans* configuration, with Ir-N and Ir-C bond distances falling in the expected ranges (**Table 1**).[45–47] The Me-Campy ligand displays notably longer Ir-N distances, which can be attributed to the *trans*-influence of the strong Ir-C bonds of the ppy ligands. With reference to the chiral carbon atom on the Me-Campy ligand, the assignment of its configurations is the *R* one, according to the Cahn-Ingold-Prelog convention. The five membered chelate ring defined by the Me-Campy ligand at the Ir(III) metal centre is not planar. According to the ring puckering analysis of PLATON,[48] the metallacycle conformation is better described as an envelope form on N(3).[49] By using the same ring puckering parameters, the C6-ring of the tetrahydroquinoline moiety shows a conformation very close to an half-chair, being the Θ and ϕ parameters 51.1(6) and 65.0(7)°, respectively, with the C(24) atom about 0.7 Å out of the mean plane passing through the C(23), C(25), C(26), C(27) and C(31) carbon atoms. In analogy with similar Ir(III) ppy derivatives containing ethylendiamine and picolylamine as ancillary N,N chelated ligands, the supramolecular organization of Ir-Me-Campy is mainly built up through intermolecular interactions involving the NH_2 functionality of the Me-Campy ligand and the chloride anion. Indeed, the supramolecular building is sustained by N-H···Cl interactions [N(3)•••Cl^i distance: 3.284(3) Å, N(3)-H(3b)•••$Cl(1)^i$ and angle: 2.47 Å and 150°, respectively; i = x, y, z] and C-H···Cl interactions with the ppy hydrogen atoms in meta position with respect to both the coordinated N and C atoms [C(4)-H(4)···Cl^{ii} distance: 2.80 Å and angle: 175°; C(7)-H(7)···$Cl(1)^{ii}$ distance: 2.88 Å and angle: 179°, with ii = 1/2-x+1, -y, z-1/2]. Moreover, the co-crystallized water molecule is anchored next to both the metal cation and the chloride counterion through an heteroatom···halogen contact,[50] where chloride interacts noncovalently to the electronegative oxygen atom at distance: 3.258(1) Å.

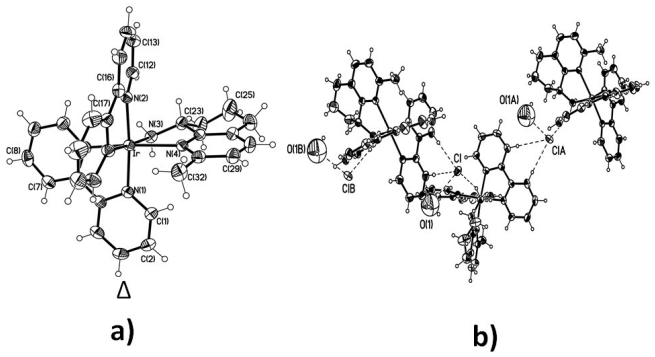

Fig. 1 View of the Δ form in the metal cation of **Ir-Me-Campy** showing the atomic labelling scheme (**a**) and the perspective view of the 1D supramolecular motif of **Ir-Me-Campy** showing the anion intermolecular interactions (**b**).

3.2 Chiroptical properties: VCD results

In **Figure 2** on the left we superimpose the experimental VCD (top) and IR absorption spectra of Δ*S*-Ir-Me-Campy and of Λ*R*-Ir-Me-Campy and on the right we superimpose the experimental VCD and IR spectra of Δ*R*-Ir-Me-Campy and Λ*S*-Ir-Me-Campy. In **Figure 3** on the left we report the experimental VCD and IR spectra of Λ*R*-Ir-H-Campy, while on the right we report the experimental VCD and IR spectra of Λ*S*-Ir-H-Campy. Interestingly the VCD spectra of the enantiomeric couple of the left panel of **Figure 2** are rather different from the VCD spectra of the diastereomerically related enantiomeric couple in the right panel of the same Figure, whereas the IR spectra show no appreciable difference; in other cases an analogous situation with quite indistinguishable absorption spectra of diastereoisomers had already been observed, for example when planar and central chirality were co-present.[29] It is also interesting to notice a good correspondence of the VCD data of Ir-H-Campy (**Figure 3**) with the VCD data of Ir-Me-Campy (**Figure 2**) for cases endowed with the same chirality at the metal centre (once more the IR spectra of **Figure 3** are quite similar to the spectra of **Figure 2**).

Considering a detailed comment of results of **Figure 2**, we ob-

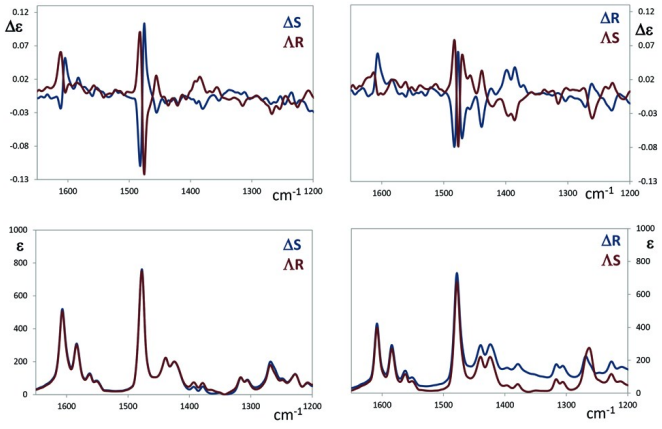

Fig. 2 Superimposed experimental Vibrational Circular Dichroism (VCD) (top panels) and IR (lower panels) spectra of Δ*S*-Ir-Me-Campy and of Λ*R*-Ir-Me-Campy (left) and superimposed experimental VCD and IR of Δ*R*-Ir-Me-Campy and of Λ*S*-Ir-Me-Campy (right). Notice the colour code for the spectra: blue for Δ-isomers and red for Λ-isomers.

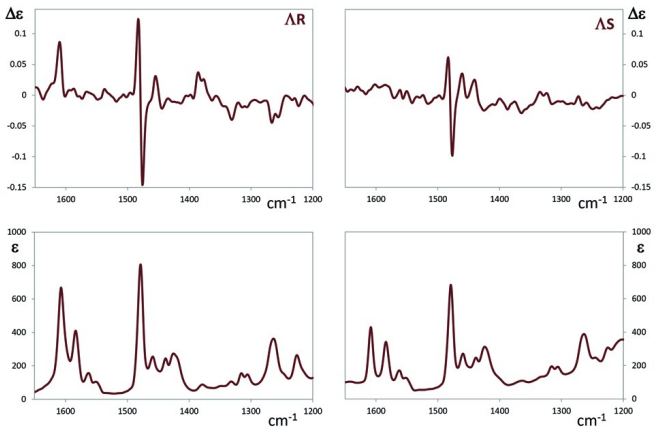

Fig. 3 Experimental Vibrational Circular Dichroism (VCD) (top panels) and IR (lower panels) spectra of Λ*R*-Ir-Campy (left) and of Λ*S*-Ir-Campy (right). Please notice that the colour of all spectra is red, since all species are Λ.

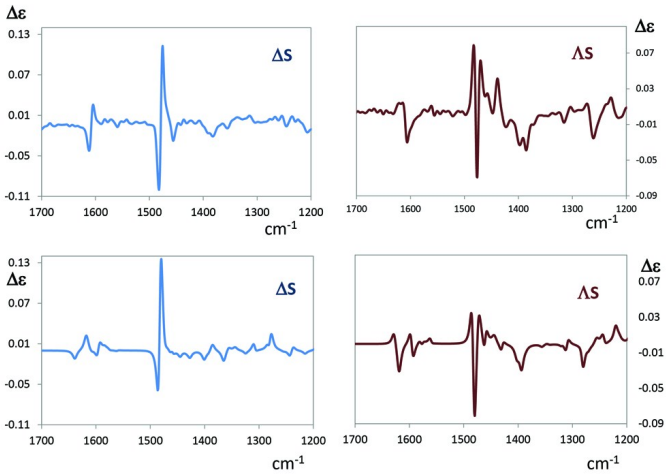

Fig. 4 Comparison of calculated (top) and experimental (lower) VCD spectra of Δ*S*-Ir-Me-Campy (left in blue) and of Λ*S*-Ir-Me-Campy (right in red). DFT calculated spectra are for X-ray optimized structures (see text for more details).

serve that:

i) Two doublets with alternating signs are present in the VCD spectra of Ir-Me-Campy (**Figure 2**) at ca. 1600 cm^{-1} and at 1475 cm^{-1} (the latter doublet is somewhat concealed by a nearby VCD band at ca. 1470 cm^{-1}): the two doublets have positive chirality for the Δ-diastereomers ((+,-) in order of increasing energy/wavenumber, as defined e.g. by Harada, Berova and Nakanishi for excitons[51]) and negative chirality for the Λ-diastereomers. The sign of the doublets is independent on the configuration of the stereogenic carbon atom. The second doublet is more intense and it is observed also in the VCD spectra of Λ*R*-Ir-H-Campy and Λ*S*-Ir-H-Campy and it is negative there, since the absolute configuration at Ir is Λ. It is tempting to state that we are in presence, at least for the doublets at 1475 cm^{-1}, of *vibrational excitons*, even though they are not the usual vibrational excitons associated to C=O groups, as in the cases discussed in refs[52,53]. The intensity of the corresponding IR absorption band is quite large, and is indeed the most intense in the whole IR spectrum. The discussion of the assignment of the 1475 cm^{-1} doublet to a vibrational exciton is provided below, on the basis of DFT calculations.

ii) On the other hand one may clearly notice at ca. 1380 cm^{-1} a medium-intensity monosignate structured VCD feature which is positive for *R* diastereomers and negative for *S* diastereomers, both for Ir-Me-Campy and Ir-H-Campy independently on the Δ/Λ chirality (cfr. **Figures 2** and **3**). This is a clear proof of the powerful of the VCD method, which is able to "see" both types of chiralities, even in the case of metal-dictated chirality.

DFT calculations for Δ*S*-Ir-Me-Campy and for Λ*S*-Ir-Me-Campy help provide firmer ground to the above conclusions; the calculated VCD spectra are compared in **Figure 4** with the experimental results. We reiterate here that calculations were started on experimental X-ray derived geometries, which were thereafter optimized to achieve correct Hessian matrices. We also wish to point out that the Cl^- ion was included in the calculations and the C6-ring of the tetrahydroquinoline moiety had an half-chair conformation on C(24) (see **ESI-3** of the ESI file, for complete information). Optimization with different conformations for the tetrahydroquinoline ring suggest that boat or half-chair on C(25) structures exhibit negligible populations. Calculated spectra are pretty good in both signs and intensities. Also calculated IR spectra are in very good correspondence with the experiment (**Figure ESI-4**). The calculated geometries for Δ*S*-Ir-Me-Campy and for Λ*S*-Ir-Me-Campy are provided in **Figure 5** and are shown from an opportune perspective to better evidence the relation to each other (vide infra).

In particular one may notice that the intense doublet structure centred at ca. 1475 cm^{-1} is excellently predicted by calculations: the assignment made in **Table ESI-5** and **Table ESI-6** of ESI shows that the normal modes underlying the two components of the doublet are the symmetric (at higher frequency) and anti-symmetric (at lower frequency) combinations of in plane CC-

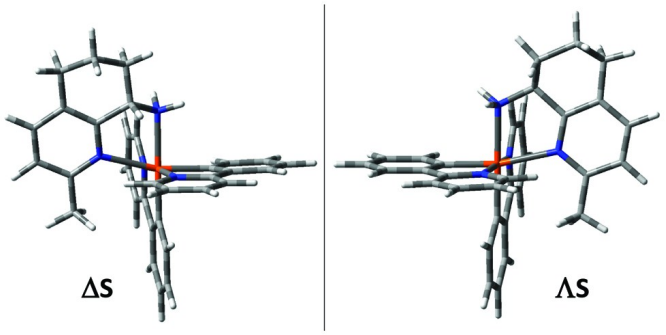

Fig. 5 Calculated structures of Δ*S*-Ir-Me-Campy (left) and of Λ*S*-Ir-Me-Campy (right)

stretching modes located on the two ppy-moieties, whose electric dipole transition moments are strong and oriented parallel to the major axis of the phenyl-pyridine groups. As of **Tables ESI-5** and **ESI-6** the modes are number 156 and 157 and calculated at 1511 and 1514 cm^{-1} (no scaling factor applied to wavenumbers), with rotational strengths equal to $+739x10^{-44}$ esu^2cm^2 (Δ*S* case)/-714 $x10^{-44}$ esu^2cm^2 (Λ*S* case) and to $-585x10^{-44}$ esu^2cm^2 (Δ*S*)/$+572$ $x10^{-44}$ esu^2cm^2 (Λ*S* case). The experimental and calculated couplets are approximately conservative and show the typical values for vibrational excitons, like the ones introduced by Taniguchi and Monde[52] and discussed later for interacting C=O stretching vibrations:[53] a more similar case to the present one has been recently reported for two interacting phenoxy moieties.[54] Further understanding of this phenomenon is attained by looking at **Figure 5**, where one may appreciate that the two couples of ppy groups coordinated to the metal in the Δ*S*-(left) and Λ*S*-cases (right) are enantiomerically related. Indeed in the Δ-case, in order to bring the ppy moiety closest to the observer (drawn horizontally in **Figure 5**) to coincide with the farthest one, one (drawn vertically in **Figure 5**) has to make a clockwise rotation (left side of the figure), and this means positive chirality; in the Λ-case instead one has to make a counter clockwise rotation (right side of the Figure) to achieve the same result, and this means negative chirality. The angle formed by the two ppy-moieties, which is the same as the angle formed by the two electric dipole transition moments, associated to each ppy-group, is closed to 90°, a situation in which the applicability of the vibrational exciton formulas to calculate rotational strengths is safe.[53] Quantitative application of the model of ref.[53] requires the electric dipole transition moment and frequency values for each one of the two isolated ppy-units: a DFT calculation was conducted on a ppy-group, which was opportunely coordinated to an isoelectronic Ir(III) atom whose coordination sphere was completed with three NH_3-molecules and a CH_3-group, as in **Figure ESI-6**. For this model the relevant normal mode was found at 1512 cm^{-1}, with dipole strength equal to 496 x 10^{-40} esu^2cm^2. For Me-Campy the inter-ppy dihedral angle was assumed to be C(phe)-C(py)-C(py)-C(phe), and this turned out to be ca. ±110°; the distance d between the two ppy-units was taken as the C(py)-C(py)-distance and the angles α_1 and α_2 as C(phe)-C(py)-C(py)(for the definition of atoms C(phe) and C(py) of each phenylpyridine unit see **Figure ESI-4**). As pointed out in ref.[53], caution must be taken to obtain the correct frequency order for the symmetric and antisymmetric modes: the calculated geometry (α_1, α_2 and dihedral angle) guarantees higher wavenumber for the symmetric normal mode. Results are given in **Table 2** and show excellent agreement between full DFT and model calculations for frequencies, dipole strengths and rotational strengths, leaving no doubt to the vibrational exciton interpretation of the doublets. Following the DFT calculations, one may understand the origin of the VCD band at ca. 1380 cm^{-1}, which is negative for *S* and positive for *R* configuration of the stereogenic carbon atom, independently on the Δ/Λ chirality. Indeed underneath that VCD band one may identify a couple of normal modes, *i.e.* 142 and 143, the rotational strength of which is about $-40x10^{-44}$ esu^2cm^2, comprising the bending vibration of the C*H, C* being the stereogenic carbon atom (please notice that the calculated frequencies for these modes are about 1430 cm^{-1}, prior to scaling factoring). The sensitiveness of C*H bending to carbon chirality has been noticed in similar circumstances in the VCD spectrum of two different molecules bearing an "external" C* in refs.[29] and[30].

Table 2 Comparison of frequencies $\nu\pm$, dipole strengths D± and rotational strengths R± for Λ*S* and Δ*S*-Me-Campy calculated by the vibrational exciton model and by full DFT computations.

	Λ*S*-Me-Campy		Δ*S*-Me-Campy	
	model	DFT	model	DFT
$\nu+^a$	1512.3	1514.0	1512.3	1514.0
$\nu-^a$	1511.7	1512.0	1511.7	1511.0
$D+^b$	267.2	253.0	249.7	308.0
$D-^b$	724.8	695.0	742.3	677.0
$R+^c$	483.1	572.0	-463.3	-585.0
$R-^c$	-482.9	-714.0	463.1	739.0
Parameter obtained from DFT calculation on *ppy*-model				
$D(10^{-40}$ $esu^2cm^2)$	496		496	
$\nu(cm^{-1})$	1512		1512	
$\phi(°)$	-108		110	
d(Å)	5.53		5.47	
$\alpha_1(°)$	62		61	
$\alpha_2(°)$	62		61	

[a] cm^{-1}, [b] 10^{-40} esu^2cm^2, [c] 10^{-44} esu^2cm^2

3.3 Chiroptical properties: CPL and ECD results

As stated earlier and reported in ref.[17], ECD spectra are informative about chirality at the metal, but not about the configuration at C*. The TDDFT calculations reported in **Figure 6** for Ir-Me-Campy systems match satisfactorily with the experimental spectra, but do not provide further information about the asymmetric carbon atom. Finally in **Figure 7** on the left we superimpose the experimental CPL (top) and fluorescence spectra of Δ*S*-Ir-Me-Campy and of Λ*R*-Ir-Me-Campy and on the right we superimpose the experimental CPL and fluorescence spectra of Δ*R*-Ir-Me-Campy and of Λ*S*-Ir-Me-Campy. In **Figure 8** on the left we reported the experimental CPL and fluorescence spectra of Λ*R*-Ir-H-Campy, while on the right we reported the experimental CPL and fluorescence spectra of Λ*S*-Ir-H-Campy. The CPL spec-

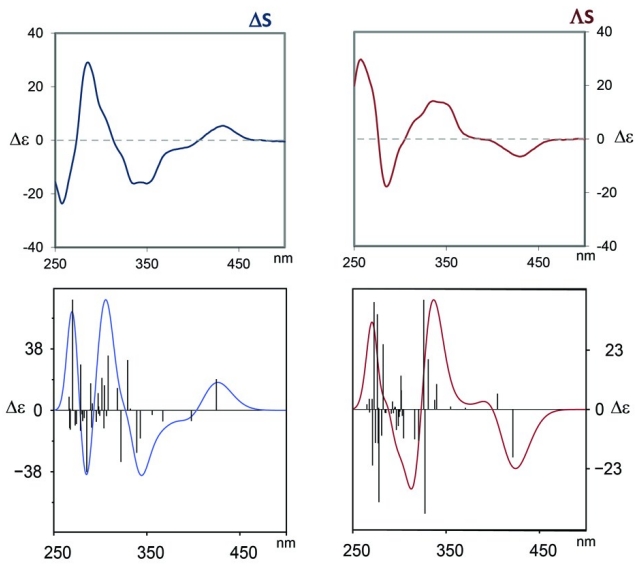

Fig. 6 Comparison of experimental (top) and calculated ECD (lower) spectra of Δ*S*-Ir-Me-Campy (left) and of Λ*S*-Ir-Me-Campy (right). DFT calculated spectra are for X-ray optimized structures (see text for more details).

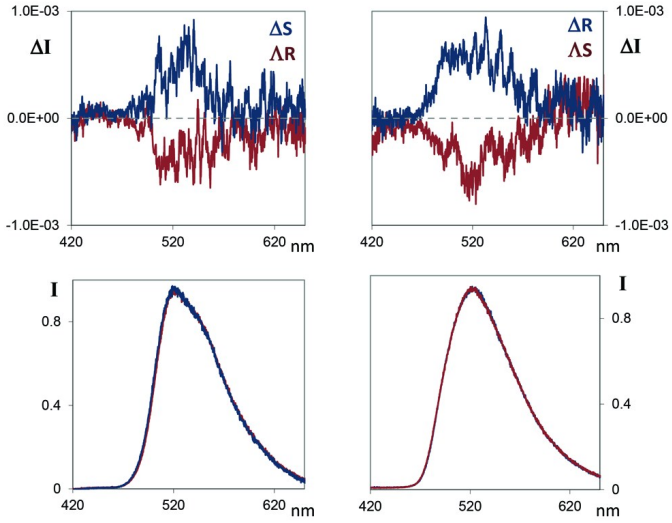

Fig. 7 Superimposed experimental Circularly Polarized Luminescence (CPL) (top panels) and total luminescence (lower panels) spectra of Δ*S*-Ir-Me-Campy and of Λ*R*-Ir-Me-Campy (left) and superimposed experimental CPL and fluorescence spectra of Δ*R*-Ir-Me-Campy and Λ*S*-Ir-Me-Campy (right).

tra in each top panel of **Figure 7** are, within experimental error, mirror-image to each other; the CPL spectra of the diastereomeric (Δ*S*,Λ*R*) and (Δ*R*,Λ*S*) couples however are not identical, as well as their fluorescence spectra. Indeed the sign and the absolute value of the g_{lum}-ratio [g_{lum} = (I_L-I_R)/ ½(I_L+I_R)](evidenced here by plotting the fluorescence spectra so as to exhibit the maximum intensity at 1) are similar in (Δ*S*,Λ*R*) and (Δ*R*,Λ*S*); in particular the sign for the CPL band of each species, + for Δ and – for Λ, is the same as the sign of the lowest energy band in the ECD spectrum. Notice also that the CPL spectra of Λ*R*-Ir-H-Campy and Λ*S*-Ir-H-Campy are both negative, as for Λ*R*-Ir-Me-Campy and Λ*S*-Ir-Me-Campy; the presence or absence of a methyl group does not influence the most relevant features of the fluorescence and CPL data. On the other hand subtle but definite differences are noticed between (Δ*S*,Λ*R*) and (Δ*R*,Λ*S*) species, possibly due to different vibronic coupling effects, as evinced also in the different shape of fluorescence spectra. The structuring of fluorescence and CPL spectra for Λ*R*-Ir-H-Campy and Λ*S*-Ir-H-Campy is less evident. In particular the g_{lum} factor is lower and the spectra are very noisy. The CPL phenomenon is mainly originated in the Δ/Λ molecular chirality. Finally we notice that the dissymmetry g_{lum} factors for Ir-Me-Campy complexes are of the order of 10^{-3}: similar values had been measured in the previously conducted works on Ir complexes.[16,31,32] DFT calculations are outside our reach now, since, rather convincingly, it has been put forward that the phosphorescence band in this case be due to T_1->S_0 transition.[55]

4 Conclusions

In this work we have measured the VCD spectra of Δ,Λ-*(R,S)*-[(ppy)$_2$Ir(Me-campy)]X, where ppy=2-phenylpyridine, Me-campy=2-methyl-5,6,7,8-tetrahydroquinolin-8-amine, and the complex Λ-*(R,S)*-[(ppy)$_2$Ir(H-Campy)]X, where ppy=2-phenylpyridine, H-Campy=8-amino-5,6,7,8-tetrahydroquinolines and with X^- = Cl^- as counterion. In the VCD spectra have been highlighted the spectroscopic signatures for both types of chiralities, suggesting a good sensitivity of this chiroptical method to discriminate the diastereomers. Indeed we were able to identify strong structural significance in the VCD doublet observed at ca. 1475 cm^{-1}, which turns out to be the signature for chirality at the metal. Indeed this doublet, which is a vibrational exciton doublet[52–54], is generated by the two phenyl pyridine groups directly coordinated to the metal: when the two ppy-groups form a positive helicity moiety, as in Δ-complexes, a positive vibrational exciton (+,- from low to high frequencies) is generated and observed; otherwise when the two ppy-groups form a negative helicity moiety, as in Λ-complexes, a negative vibrational exciton is generated and observed. Such a strong and simple picture is not emerging from ECD data, due to the superposition of many electronic transitions; furthermore no specific signature for central C* chirality is evident in ECD spectra. The latter one instead is manifested in the VCD spectra, around 1380 cm^{-1}, with features associated to C*H bending. Finally CPL spectra were recorded for the same systems in solution; differences for (Δ*S*,Λ*R*) and (Δ*R*,Λ*S*) species were noticed. Their interpretation, which can be relevant to understand the optical properties of these systems, represents a challenge for theory and calculations as well.[55]

References

1 Y. You and W. Nam, *Chem. Soc. Rev.*, 2012, **41**, 7061–7084.
2 M. K. Nazeeruddin, C. Klein, M. Grätzel, L. Zuppiroli and D. Berner, in *Highly Effic. OLEDs with Phosphorescent Mater.*, Wiley-VCH Verlag GmbH & Co. KGaA, 2008, pp. 363–390.
3 Z.-q. Chen, Z.-q. Bian and C.-h. Huang, *Adv. Mater.*, 2010, **22**, 1534–9.

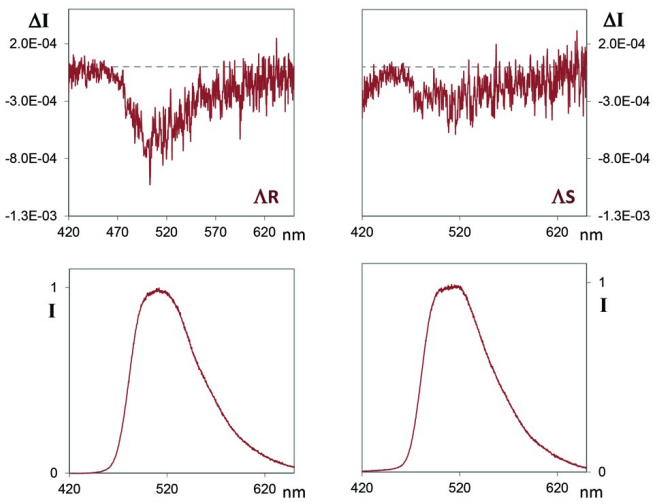

Fig. 8 Experimental Circularly Polarized Luminescence (top panels) and fluorescence (lower panels) spectra of Λ*R*-Ir-H-Campy (left) and of Λ*S*-Ir-H-Campy (right).

4 C. Ulbricht, B. Beyer, C. Friebe, A. Winter and U. S. Schubert, *Adv. Mater.*, 2009, **21**, 4418–4441.

5 L. Lu, M. Wang, L.-J. Liu, C.-Y. Wong, C.-H. Leung and D.-L. Ma, *Chem. Commun.*, 2015, **51**, 9953–9956.

6 P. Göbel, F. Ritterbusch, M. Helms, M. Bischof, K. Harms, M. Jung and E. Meggers, *Eur. J. Inorg. Chem.*, 2015, **2015**, 1654–1659.

7 F. Xue, Y. Lu, Z. Zhou, M. Shi, Y. Yan, H. Yang and S. Yang, *Organometallics*, 2015, **34**, 73–77.

8 Y. You, *Curr. Opin. Chem. Biol.*, 2013, **17**, 699–707.

9 T. Yoshihara, M. Hosaka, M. Terata, K. Ichikawa, S. Murayama, A. Tanaka, M. Mori, H. Itabashi, T. Takeuchi and S. Tobita, *Anal. Chem.*, 2015, **87**, 2710–2717.

10 Q. Zhao, C. Huang and F. Li, *Chem. Soc. Rev.*, 2011, **40**, 2508–2524.

11 K. K.-W. Lo and K. Y. Zhang, *RSC Adv.*, 2012, **2**, 12069–12083.

12 K. K.-W. Lo, M.-W. Louie and K. Y. Zhang, *Coord. Chem. Rev.*, 2010, **254**, 2603–2622.

13 A. Auffrant, A. Barbieri, F. Barigelletti, J. Lacour, P. Mobian, J.-P. Collin, J.-P. Sauvage and B. Ventura, *Inorg. Chem.*, 2007, **46**, 6911–6919.

14 M. Helms, Z. Lin, L. Gong, K. Harms and E. Meggers, *Eur. J. Inorg. Chem.*, 2013, **2013**, 4164–4172.

15 E. Marchi, R. Sinisi, G. Bergamini, M. Tragni, M. Monari, M. Bandini and P. Ceroni, *Chem. – A Eur. J.*, 2012, **18**, 8765–8773.

16 M. Ashizawa, L. Yang, K. Kobayashi, H. Sato, A. Yamagishi, F. Okuda, T. Harada, R. Kuroda and M.-a. Haga, *Dalt. Trans.*, 2009, 1700–1702.

17 L. Ricciardi, M. La Deda, A. Ionescu, N. Godbert, I. Aiello, M. Ghedini, M. Fusè, I. Rimoldi and E. Cesarotti, *J. Lumin.*, 2015, LUMIND1500684, doi/10.1016/j.jlumin.2015.08.003.

18 L. A. Nafie, *Vibrational Optical Activity*, John Wiley & Sons, Ltd, 2011.

19 T. Keiderling, in *Circ. Dichroism Princ. Appl.*, 2000, pp. 621–666.

20 P. L. Polavarapu and C. Zhao, *Fresenius. J. Anal. Chem.*, 2000, **366**, 727–734.

21 P. L. Polavarapu, J. Frelek and M. Woźnica, *Tetrahedron: Asymmetry*, 2011, **22**, 1720–1724.

22 T. Buffeteau, L. Ducasse, A. Brizard, I. Huc and R. Oda, *J. Phys. Chem. A*, 2004, **108**, 4080–4086.

23 G. Yang and Y. Xu, in *Electron. Magn. Prop. Chiral Mol. Supramol. Archit. SE - 86*, ed. R. Naaman, D. N. Beratan and D. Waldeck, Springer Berlin Heidelberg, 2011, vol. 298, pp. 189–236.

24 S. Abbate, L. F. Burgi, F. Gangemi, R. Gangemi, F. Lebon, G. Longhi, V. M. Pultz and D. A. Lightner, *J. Phys. Chem. A*, 2009, **113**, 11390–11405.

25 S. R. Domingos, M. R. Panman, B. H. Bakker, F. Hartl, W. J. Buma and S. Woutersen, *Chem. Commun.*, 2012, **48**, 353–355.

26 S. R. Domingos, A. Huerta-Viga, L. Baij, S. Amirjalayer, D. A. E. Dunnebier, A. J. C. Walters, M. Finger, L. A. Nafie, B. de Bruin, W. J. Buma and S. Woutersen, *J. Am. Chem. Soc.*, 2014, **136**, 3530–3535.

27 C. Merten, K. Hiller and Y. Xu, *Phys. Chem. Chem. Phys.*, 2012, **14**, 12884–12891.

28 M. Fuse, G. Mazzeo, G. Longhi, S. Abbate, D. Zerla, I. Rimoldi, A. Contini and E. Cesarotti, *Chem. Commun.*, 2015, **51**, 9385–9387.

29 S. Abbate, F. Lebon, S. Lepri, G. Longhi, R. Gangemi, S. Spizzichino, G. Bellachioma and R. Ruzziconi, *ChemPhysChem*, 2011, **12**, 3519–3523.

30 G. Mazzeo, G. Longhi, S. Abbate, F. Buonerba and R. Ruzziconi, *European J. Org. Chem.*, 2014, **2014**, 7353–7363.

31 F. J. Coughlin, M. S. Westrol, K. D. Oyler, N. Byrne, C. Kraml, E. Zysman-Colman, M. S. Lowry and S. Bernhard, *Inorg. Chem.*, 2008, **47**, 2039–2048.

32 C. Schaffner-Hamann, A. von Zelewsky, A. Barbieri, F. Barigelletti, G. Muller, J. P. Riehl and A. Neels, *J. Am. Chem. Soc.*, 2004, **126**, 9339–9348.

33 Bruker Analytical X-ray Systems Inc, *SAINT, Version 6.45 Copyright (c)*, 2003.

34 G. Sheldrick and . Bruker AXS Inc., Madison, WI, USA, *SADABS. Version 2.10*.

35 Bruker Analytical X-ray Systems Inc, *SHELXTL-NT, Version 5.1 Copyright (c)*, 1999.

36 E. Castiglioni, S. Abbate and G. Longhi, *Appl. Spectrosc.*, 2010, **64**, 1416–1419.

37 G. Longhi, E. Castiglioni, S. Abbate, F. Lebon and D. A. Lightner, *Chirality*, 2013, **25**, 589–599.

38 S. Abbate, G. Longhi, F. Lebon, E. Castiglioni, S. Superchi, L. Pisani, F. Fontana, F. Torricelli, T. Caronna, C. Villani, R. Sabia, M. Tommasini, A. Lucotti, D. Mendola, A. Mele and D. A. Lightner, *J. Phys. Chem. C*, 2014, **118**, 1682–1695.

39 M. J. Frisch, G. W. Trucks, H. B. Schlegel, G. E. Scuseria, M. A. Robb, J. R. Cheeseman, G. Scalmani, V. Barone,

B. Mennucci, G. A. Petersson, H. Nakatsuji, M. Caricato, X. Li, H. P. Hratchian, A. F. Izmaylov, J. Bloino, G. Zheng, J. L. Sonnenberg, M. Hada, M. Ehara, K. Toyota, R. Fukuda, J. Hasegawa, M. Ishida, T. Nakajima, Y. Honda, O. Kitao, H. Nakai, T. Vreven, J. A. Montgomery, Jr., J. E. Peralta, F. Ogliaro, M. Bearpark, J. J. Heyd, E. Brothers, K. N. Kudin, V. N. Staroverov, R. Kobayashi, J. Normand, K. Raghavachari, A. Rendell, J. C. Burant, S. S. Iyengar, J. Tomasi, M. Cossi, N. Rega, J. M. Millam, M. Klene, J. E. Knox, J. B. Cross, V. Bakken, C. Adamo, J. Jaramillo, R. Gomperts, R. E. Stratmann, O. Yazyev, A. J. Austin, R. Cammi, C. Pomelli, J. W. Ochterski, R. L. Martin, K. Morokuma, V. G. Zakrzewski, G. A. Voth, P. Salvador, J. J. Dannenberg, S. Dapprich, A. D. Daniels, . Farkas, J. B. Foresman, J. V. Ortiz, J. Cioslowski and D. J. Fox, *Gaussian 09 Revision D.01*, Gaussian Inc. Wallingford CT 2009.

40 G. Szilvágyi, B. Brém, G. Báti, L. Tölgyesi, M. Hollósi and E. Vass, *Dalt. Trans.*, 2013, **42**, 13137–44.

41 C. Merten and Y. Xu, *Dalt. Trans.*, 2013, **42**, 10572–10578.

42 Z. Dezhahang, M. R. Poopari, J. Cheramy and Y. Xu, *Inorg. Chem.*, 2015, **54**, 4539–49.

43 J. Tomasi, B. Mennucci and R. Cammi, *Chem. Rev.*, 2005, **105**, 2999–3094.

44 P. J. Stephens, *J. Phys. Chem.*, 1985, **89**, 748–752.

45 T. F. Mastropietro, Y. J. Yadav, E. I. Szerb, A. M. Talarico, M. Ghedini and A. Crispini, *Dalt. Trans.*, 2012, **41**, 8899.

46 A. M. Talarico, I. Aiello, A. Bellusci, A. Crispini, M. Ghedini, N. Godbert, T. Pugliese and E. Szerb, *Dalt. Trans.*, 2010, **39**, 1709–1712.

47 A. M. Talarico, E. I. Szerb, T. F. Mastropietro, I. Aiello, A. Crispini and M. Ghedini, *Dalt. Trans.*, 2012, **41**, 4919.

48 Utrecht University, Utrecht, The Netherlands and A. L. Spek, *PLATON, A Multipurpose Crystallographic Tool*, 1998.

49 D. G. Evans and J. C. A. Boeyens, *Acta Crystallogr. Sect. B*, 1989, **45**, 581–590.

50 A. Mukherjee, S. Tothadi and G. R. Desiraju, *Acc. Chem. Res.*, 2014, **47**, 2514–2524.

51 N. Harada, K. Nakanishi and N. Berova, in *Compr. Chiroptical Spectrosc.*, John Wiley & Sons, Inc., 2012, pp. 115–166.

52 T. Taniguchi and K. Monde, *J. Am. Chem. Soc.*, 2012, **134**, 3695–3698.

53 S. Abbate, G. Mazzeo, S. Meneghini, G. Longhi, S. E. Boiadjiev and D. A. Lightner, *J. Phys. Chem. A*, 2015, **119**, 4261–4267.

54 S. Abbate, G. Longhi, G. Mazzeo, E. Castiglioni, S. E. Boiadjiev and D. A. Lightner, Chirality 2014 Conference, Prague, 2014, pp. Note SC–28.

55 F. Monti, A. Baschieri, I. Gualandi, J. J. Serrano-Pérez, J. M. Junquera-Hernández, D. Tonelli, A. Mazzanti, S. Muzzioli, S. Stagni, C. Roldan-Carmona, A. Pertegás, H. J. Bolink, E. Ortí, L. Sambri and N. Armaroli, *Inorg. Chem.*, 2014, **53**, 7709–7721.

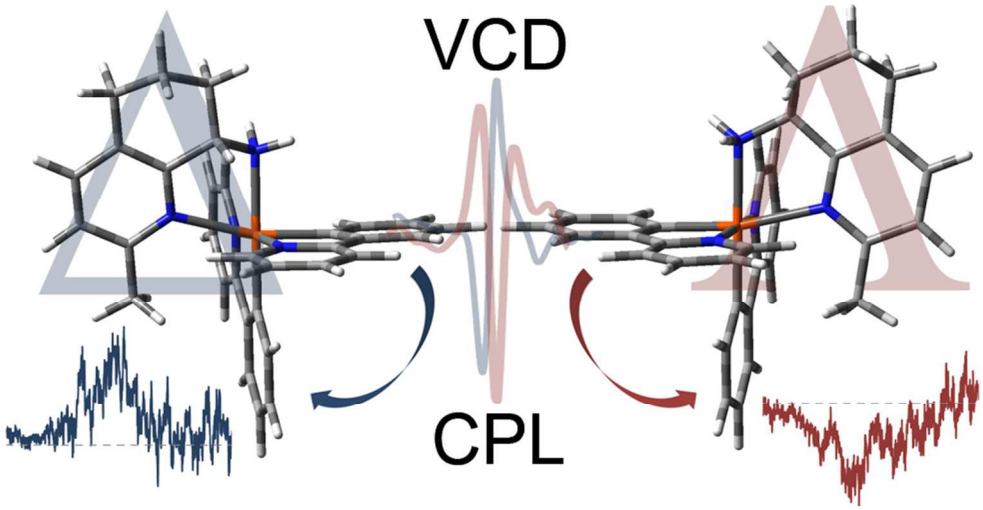

Three chiroptical spectroscopies are used on an octahedral Iridium complex. The Vibrational Exciton interpretation of VCD spectra is especially important.
84x60mm (300 x 300 DPI)